Exploration of Conduction and Stopping Power Models for Hybrid Fluid-Kinetic Simulations

LLE Summer High School Program

Aditya Srinivasan

Summer 2021

Advisors: Professor Adam Sefkow and Mike Lavell

Abstract

Radiation fluid-dynamic simulations use material models to describe the physical properties of a plasma for applications such as inertial confinement fusion. In contrast, a kinetic model can treat a wider variety of plasmas and does not need material models as long as particle collisions are treated correctly. The hybrid fluid-kinetic code TriForce uses both fluid and kinetic particles simultaneously and has collision algorithms in development to treat their interaction. The kinetic part of TriForce was used to calculate first-principles material properties such as electrical conductivity and stopping power. These calculations were used to verify the code against previous predictions by Perez et al. [Phys. Plasmas 19, 0831904 (2012)]. To calculate the conductivity of copper, an electric field was applied externally and caused the electrons to drift and conduct current. A Python code was written to calculate the conductivity based on the evolution of the electron velocity in the simulation. To calculate the stopping power, a mono-energetic beam of charged particles was launched onto a plasma at the desired density and temperature. The stopping power was then determined from the change in kinetic energy over time. Results presented in this work compare very well with analytic calculations for electrical conductivity and stopping power. This work demonstrates that the improved Monte Carlo collision algorithms in TriForce model elastic collisions well. Therefore, calculations like those presented here can be reliable inputs to TriForce (or any other fluid code) in the fluid regime. Alternately, electrical conductivity and stopping power can be calculated in-line when TriForce is used in the kinetic regime.

1 Introduction

Inertial Confinement Fusion (ICF) is a potential source of clean and unlimited energy. Since fusion involves materials with lower atomic numbers than nuclear fission, both the input fuel and the waste products are not (or much less) radioactive. This is a key difference from nuclear fission and makes fusion a very attractive source for energy.

Fusion energy requires very high temperatures and a typical simulation and experiment involves a range of densities, from a fraction of solid density to many times solid density. At these high temperatures the fusion fuel exists as a plasma, which is super heated matter existing as a combination of electrons, ions, and neutral atoms. Properties of these plasmas are important to model in order to predict conditions under which ICF can be an energy source.

Several attempts at proof-of-principle experiments are ongoing on large-scale facilities around the world such as the National Ignition Facility (NIF) [1] at the Lawrence Livermore National Laboratory and the OMEGA [2] laser at the University of Rochester. In ICF, a pellet containing a fuel made of isotopes of hydrogen – deuterium and tritium – is imploded using either lasers [3], [4], [5] or magnetic fields [6]. Shown below in Figure 1 is the example of laser direct drive [3], [5]. The pellet material, also known as the ablator, is typically made of polystyrene (a carbon and hydrogen plastic – shown in the pie chart on the bottom left of Figure 1). The laser irradiates the polystyrene (Figure 1 – top left), imploding the fuel (Figure 1 – middle), which compresses to high densities (Figure 1 - bottom right). The fuel is said to have ignited when the energy in the fusion reactions of the deuterium-tritium is greater than the laser energy used to irradiate the capsule. In indirect drive, being pursued on the NIF, the capsule is driven instead by x-rays that are emitted from a hohlraum (a cylindrical cavity) that is irradiated by the laser. The x-rays drive the capsule. Indirect drive [4] has achieved near-ignition in August of 2021 and experiments are ongoing to get closer to ignition. Direct-drive ignition has been predicted to be possible at the NIF but several uncertainties remain in these predictions and to date direct-drive ignition experiments have not been attempted.

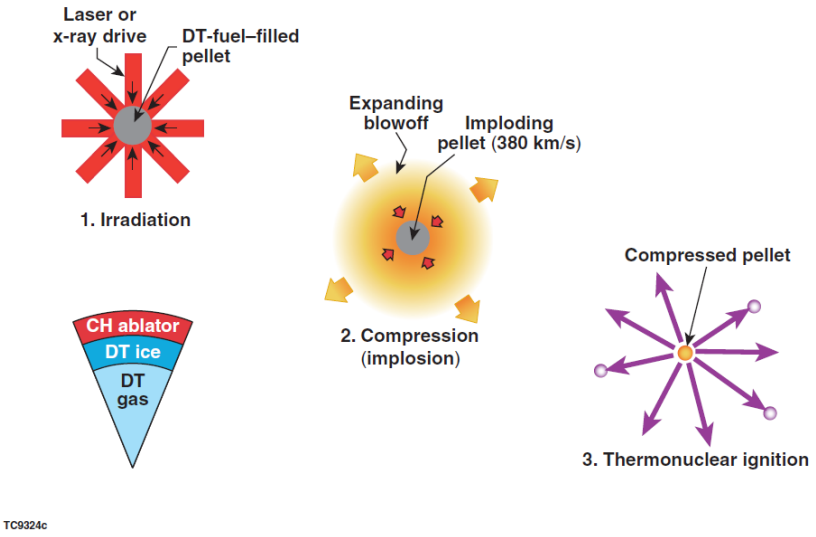

Figure 1: Schematic of laser direct drive. Step 1: A pellet made of polystyrene (CH) containing deuterium-tritium (DT) is irradiated by a laser. Step 2: The imploding pellet creates conditions suitable for fusion reactions of deuterium and tritium. Step 3: The hot, compressed core produces energy from fusion reactions. The process is similar for indirect drive, where the pellet is driven by x-rays rather than laser beams.

In this work the kinetic part of the TriForce [7] code (named TFLink) is used to calculate two transport properties of charged particles - electrical conductivity and stopping power. TriForce is a hybrid fluid-kinetic code that uses particle-based methods to calculate Coulomb collisions. Usually the plasma is approximated as a fluid and electrical properties are ignored in order to make implosion calculations more tractable. However, it is unclear as to whether this is a good approximation as such fluid codes do not reproduce experiments in all their details. In this paper, calculations are compared to previous numerical and analytic calculations from [8], with the primary goal of verifying the collision models in TriForce against this previous work.

The paper is organized as follows: in Section 2, the procedure for calculating the electrical conductivity and stopping power is described. Results are also described in the same section. Conclusions are presented in Section 3. Future work is described in Section 4.

2 Method and Results

2.1 Electrical Conductivity

The first part of this work involved determining the electrical conductivity of a copper plasma at a particular chosen density for a range of temperatures. Copper was chosen as calculations have been presented for this material in previous work [8]. The electrical conductivity was determined at one particular temperature using the steps as laid out in the flow chart in Figure 2. The same process was then employed to calculate the conductivity at other temperatures.

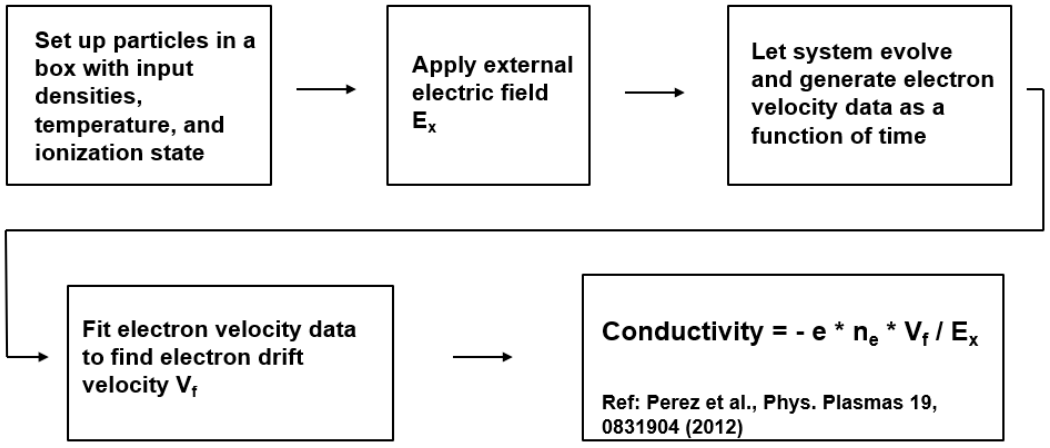

Figure 2: Process to determine the electrical conductivity using TriForce and known equations. e is the magnitude of the electron charge and n_e is the number of electrons per unit volume.

First, using the kinetic part of the TriForce code, a box of copper ions of size 1 cm $\times$ 1 cm $\times$ 1 cm with 40,000 particles was created at a particular temperature and density. This number of 40,000 was chosen to enable comparison with the calculations presented in [8], where the same number was chosen. Periodic boundary conditions were used for the box, meaning that if electrons exit one face of the box, they re-enter through the opposite face. A time step of $\Delta t = 2.5 \times 10^{-18} s$ is chosen for the problem. A self-consistent effective charge $< Z >$, calculated using an atomic model based on the Thomas-Fermi method, was also used [9]. The values used for the range of densities and temperatures are shown in Table 1 below.

n_i (1/cm^3)	kT (eV)	< Z >	n_e (1/cm^3)
8.49 x 10^{22}	1	4.6	3.90E+23
8.49 x 10^{22}	2	4.6	3.90E+23
8.49 x 10^{22}	5	4.6	3.90E+23
8.49 x 10^{22}	10	4.7	3.99E+23
8.49 x 10^{22}	20	5.2	4.42E+23
8.49 x 10^{22}	50	7.2	6.11E+23
8.49 x 10^{22}	100	9.8	8.32E+23
8.49 x 10^{22}	200	13.5	1.15E+24
8.49 x 10^{22}	500	19.8	1.68E+24
8.49 x 10^{22}	1000	24.1	2.05E+24

Table 1: Table showing the chosen ion density, n_i, the plasma temperature T (k is Boltzmann's constant), the calculated effective-charge values for a copper plasma $< Z >$, and the electron density defined by $n_e =< Z > n_i$.

Next, after setting up the particles in the box, an external electric field E_X of 3×10^{10} V/m was applied. (The value of this field is used in [8].) Third, this system was allowed to evolve naturally including the effect of electron-electron and electron-ion collisions. The electrons initially accelerate. Then collisions alter the evolution of the electron velocities until an equilibrium value is reached. The average electron velocity was recorded as a function of time. Figure 3 shows the average velocity versus time for 50 eV, 200 eV, and 500 eV initial temperatures. The electron velocities show the expected behavior of particles not in equilibrium, with an initial acceleration followed by a saturation due to the balance of Coulomb scattering and acceleration. Using these curves, it is possible to determine the final drift velocity, which is equal to the asymptotic average electron velocity at equilibrium.

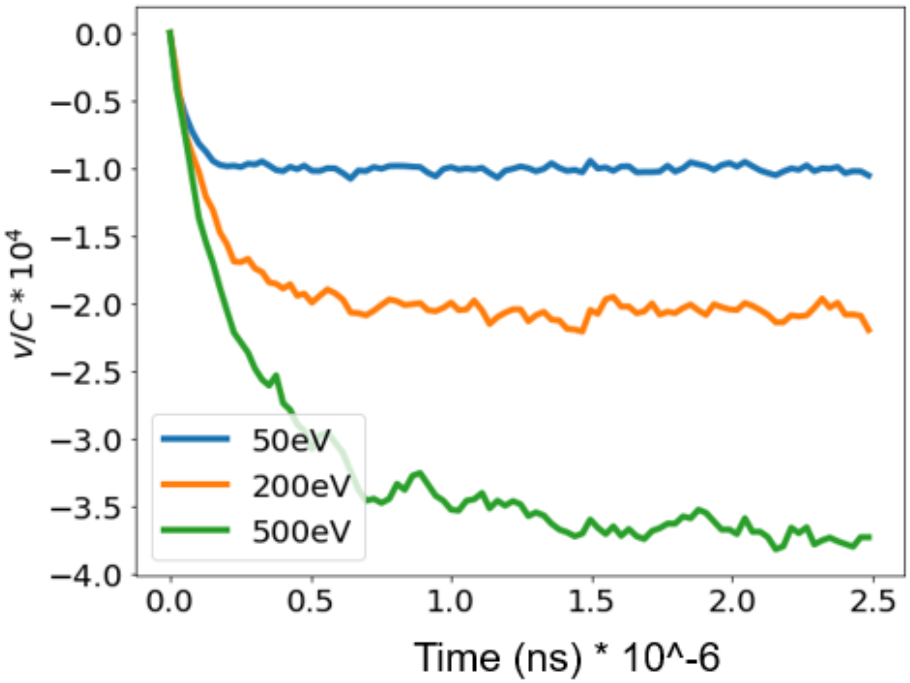

Figure 3: The ratio of the electron drift velocity, v to the speed of light, c, for 50 eV, 200 eV, and 500 eV plasmas when an electric field of 3×10^{10} V/m is applied.

To quantify the electron drift velocity, the average velocity evolution is fit to a previously identified (equation 24 in Ref. [8]) functional form for each temperature and is given by,

$$V(t) = At + V_f(1 - e^{(-t/\tau)}) \tag{1}$$

where A, V_f, and τ are fitting parameters and t is the simulation time, and V_f is the final (asymptotic) electron drift velocity. Note that this equation is valid only within the simulation time up to 2.5×10^{-15} s. Extrapolating this function to $t \to \infty$ does not have any physical meaning as it diverges.

As an example of the fitting, this functional form compared with the calculations is shown for a 200 eV temperature in Figure 4. In this figure the dimensionless ratio of the electron velocity to the light speed is shown as a function of the dimensionless time $t/\Delta t$, where Δt, the time-step is previously defined as $2.5 \times 10^{-18} s$. An excellent

fit is obtained with this functional form ($R^2 = 0.979$). Note that an asymptotic value of $v_f \sim 2 \times 10^{-4} c$ is obtained for this temperature.

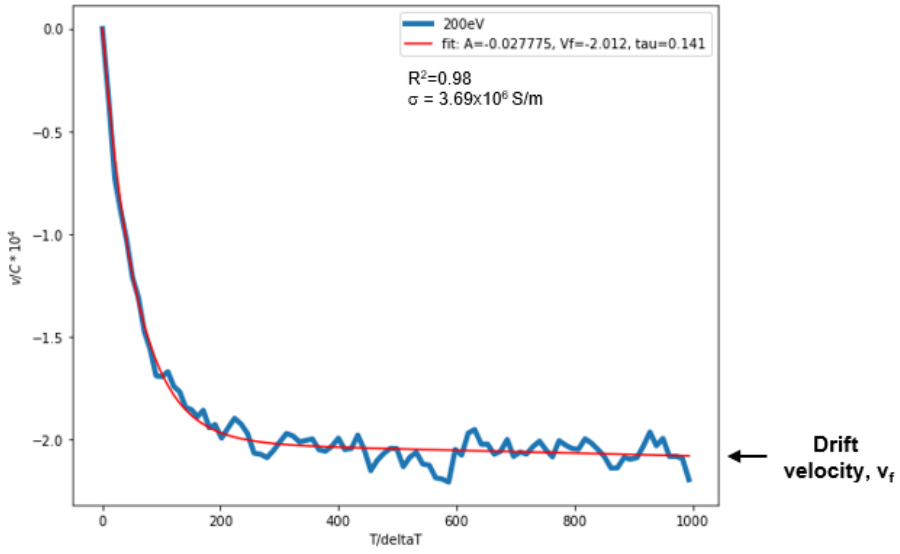

Figure 4: Ratio of the drift velocity to the speed of light for 200 eV compared to the fitting functional form given by Equation 1. The x-axis is plotted in terms of the dimensionless time, the ratio of the simulation time to the time-step in the calculation.

With this value of the drift velocity, the electrical conductivity for each temperature is given by:

$$\sigma = -e * n_e * V_f / E_x \tag{2}$$

where e represents the charge of an electron and n_e represents the number density of electrons given in Table 1.

These calculations are repeated for a range of temperatures: 1, 2, 5, 10, 20, 50, 100, 200, 500, and 1000 eV. The calculated electrical conductivity is shown in Figure 5. The blue curve shows the calculations using TriForce. In orange are the calculations using the analytic expression given by Equation 26 from Ref.[8], which is shown below:

$$\sigma = \frac{8\pi\epsilon_0 c}{r_e}\left[\frac{2 < Z >}{3\pi\bar{l}^2\sqrt{\overline{T_e}}}[1-(1+a)e^{-a}] + \frac{\overline{T}_e^{3/2}}{< Z > ln\Lambda}(1+a+\frac{a^2}{2}+\frac{a^3}{6})e^{-a}\right] \tag{3}$$

where r_e is the classical electron radius defined as $r_e = e^2/4\pi\epsilon_0 m_e c^2$, ϵ_0 is the vacuum permittivity, m_e is the electron mass, $\overline{T}_e = 2kT_e/(\pi m_e c^2)$ is the normalized temperature, $\bar{l} = (n_i r_e^3 \sqrt{3/4\pi})^{-1/3}$ is the dimensionless interatomic distance or the interatomic distance in units of r_e, $< Z >$ is the calculated effective charge, and a is the dimensionless parameter given by $a = 2 < Z > (ln\Lambda/\pi)^{1/2}/(\bar{l}\overline{T}_e)$. The Coulomb logarithm $ln\Lambda$ is given by Eq. 22 and Eq. 23 in Perez et al.

A comparison of Equation 3 and Figure 5 shows that with increasing temperatures, the conductivity is dominated by the second term in Equation 3 (the Spitzer term), which scales as $\overline{T}_e^{3/2}$. At lower temperatures, the first term, which scales as $1/\sqrt{\overline{T}_e}$, dominates the electrical conductivity.

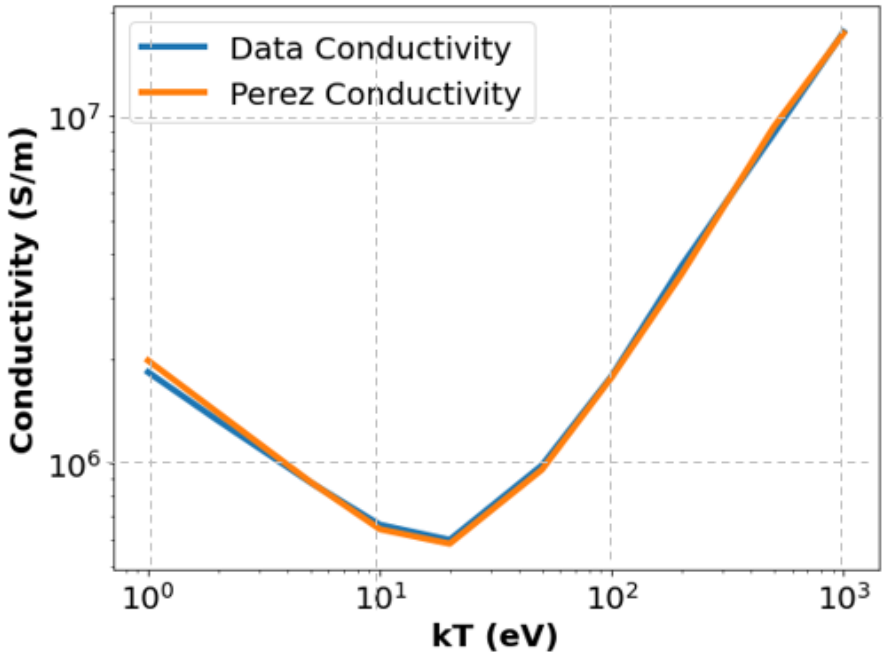

Figure 5: The calculated conductivity using TriForce (Equation 3) compared with calculations using Equation 26 in Perez et al. [8]. The similar nature of the curves indicates that TriForce's conductivity predictions are accurate.

The excellent comparison indicates that TriForce accurately calculates Coulomb collisions. These conductivity calculations can now be extended to any material under any conditions. Furthermore, it also shows that TriForce can be accurately used to

model fluid-like conditions where electrical conductivity can be an input parameter calculated from previous kinetic calculations.

2.2 Stopping power

The stopping power of a particle, defined by the change in energy of a particle per unit length, is another important transport property of charged particles in a plasma. The initial setup of the stopping power calculation was similar to the setup for the conductivity measurement. The flowchart in Figure 6 describes the steps used to calculate the stopping power.

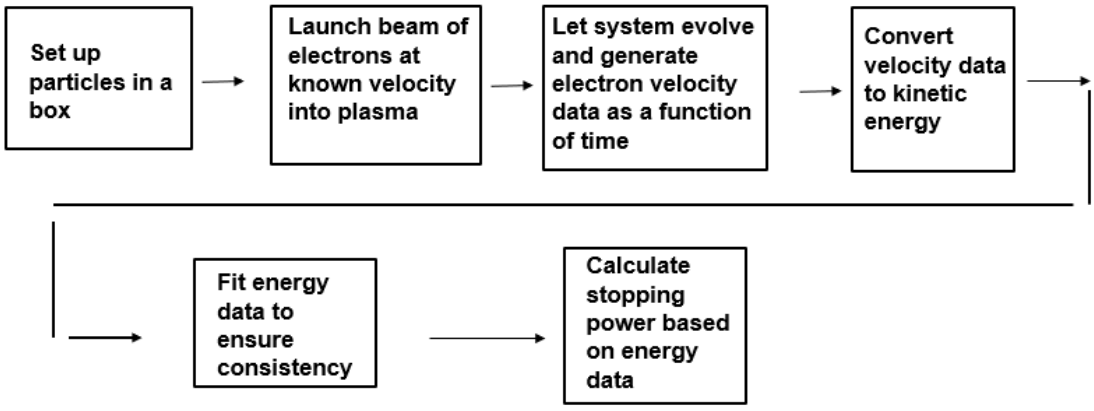

Figure 6: Process to determine the stopping power using TriForce.

Mono-energetic probe electron beams between 100 keV and 1 MeV were launched into a cold singly-ionized solid density hydrogen plasma. The cold ion plasma temperature was chosen to be 1 Kelvin so that the electron beam energies were significantly larger than the thermal plasma energy. The plasma was selected to be composed of artificially light ions (with ion mass $m_i = 5m_e$) for comparison with the plasma simulations in [8] and for easier computation.

From here, the system was allowed to evolve from its non-equilibrium state through collisions and the average beam electron velocity was recorded at each time step. Next, the velocity data was converted to kinetic energy data. Note that the standard kinetic energy velocity relationship cannot be used here since the electron beam particles move

at relativistic speeds. The relativistic momentum, p is obtained from the velocity as

$$p = \frac{m_e v}{\sqrt{1 - \frac{v^2}{c^2}}} \tag{4}$$

which is then converted to the relativistic kinetic energy as

$$E_{KE} = \sqrt{m_e^2 c^4 + p^2 c^2} - m_e c^2 \tag{5}$$

Kinetic energy curves as a function of the dimensionless ratio t/τ, where $\tau = \frac{4\pi\epsilon_0^2 m_e m_i c^3}{q_e^2 q_i^2 n_i ln\Lambda}$, are shown in Figures 7 and 8 for 1 MeV and 100 keV, respectively. q_i is the charge of the ion and q_e is the charge of the electron. Each orange line is the calculated kinetic energy as a function of time.

The analytic evolution of the beam momentum is given by Equation 27 in Perez and is given below:

$$\arctan(p') - p' - \arctan(p'_0) + p'_0 = \frac{t}{\tau} \tag{6}$$

where p' is the dimensionless mean beam momentum given by $p/m_e c = v/c\sqrt{1 - \frac{v^2}{c^2}}$ with mass = 1, p_0 is the dimensionless initial momentum, and $\tau = \frac{4\pi\epsilon_0^2 m_e m_i c^3}{q_e^2 q_i^2 n_i ln\Lambda}$. Equation 5 is used to convert the momentum to kinetic energy. These analytic curves are also shown in Figures 7 and 8.

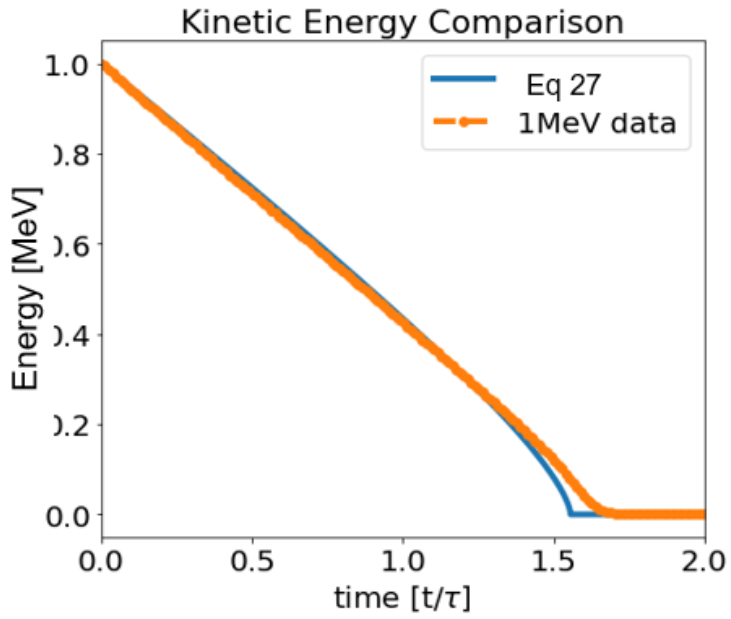

Figure 7: Calculated kinetic energy (Equation 6) from a 1 MeV beam (orange line) compared to Equation 27 in Perez (blue line) for a plasma with artificially light ions. The good comparison shows that TriForce can accurately calculate kinetic energy data.

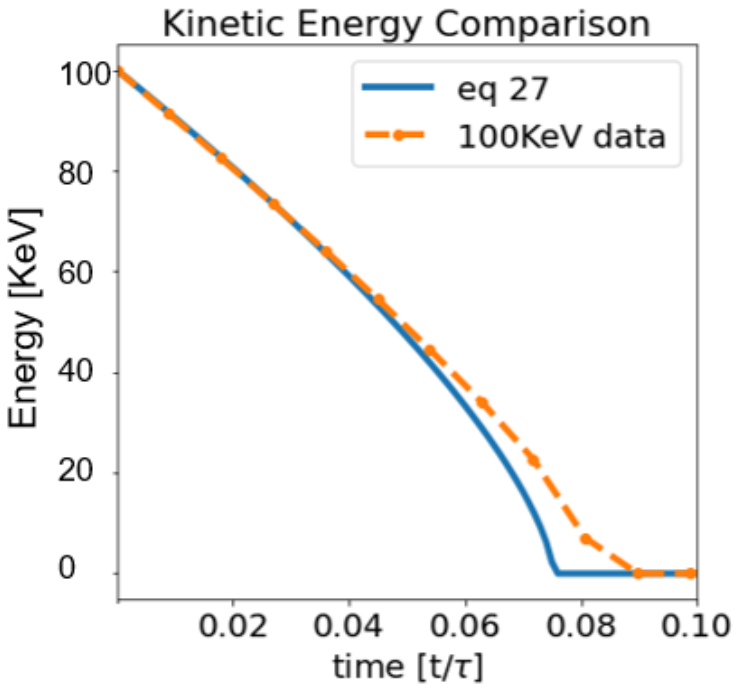

Figure 8: Calculated kinetic energy from a 100 keV beam (orange-dash line) compared to Equation 27 in Perez (blue line) for a plasma with artificially light ions. The good comparison again shows that TriForce can accurately calculate kinetic energy data.

Each blue line in the figures above is given by the conversion of the analytic equation in Equation 6 to kinetic energy using Equation 5. The similarities between the analytic and calculated kinetic energy evolution curves shows that TriForce's kinetic energy calculations reproduce the analytic formula in Equation 6, validating the electron-ion collision scheme in the code. The theory and numerical solutions diverge when the beam energy is nearly depleted because the theory solution assumes immobile ions.

Next, a more realistic and self-consistent aluminium plasma is initialized in TriForce. Probe electron beams of energies varying from 10 keV to 4 MeV are launched into this plasma in a series of calculations. Similar kinetic energy evolution (as the calculations outlined previously) is calculated as a function of time. The results for the kinetic energy evolution are summarized in Figure 9.

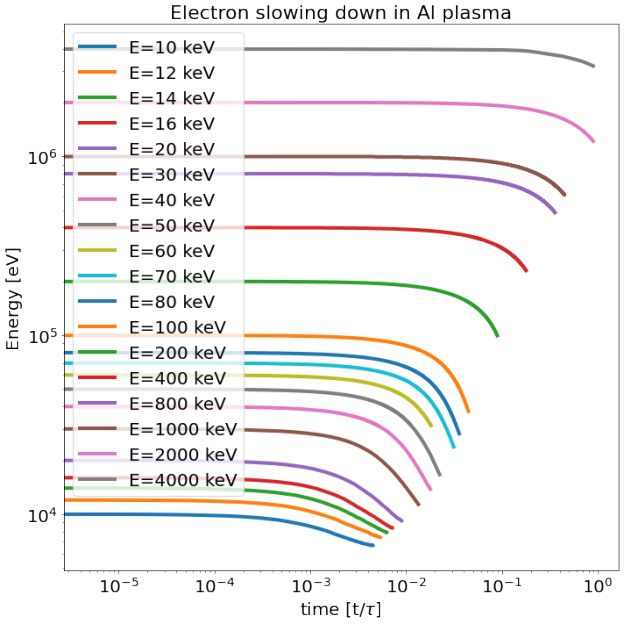

Figure 9: Kinetic energy evolution for a cold aluminum plasma for various beam energies. Note that the labels for each of the curves are listed in the opposite order, i.e., the 10 keV curve is labeled at the top but is the lowest curve in the figure.

From each of these kinetic energy curves, the stopping power (Q) can be obtained from:

$$Q = \frac{1}{v_0}\left(\frac{dE}{dt}\right)_{t=0} \tag{7}$$

where v_0 is the initial beam velocity and $(\frac{dE}{dt})_{|t=0}$ is the initial slope of the kinetic energy curve. Shown in Figure 10 is the stopping power normalized to the product of mass density in the plasma and the Coulomb logarithm (defined in Equation 23 in [8]) versus the electron energy.

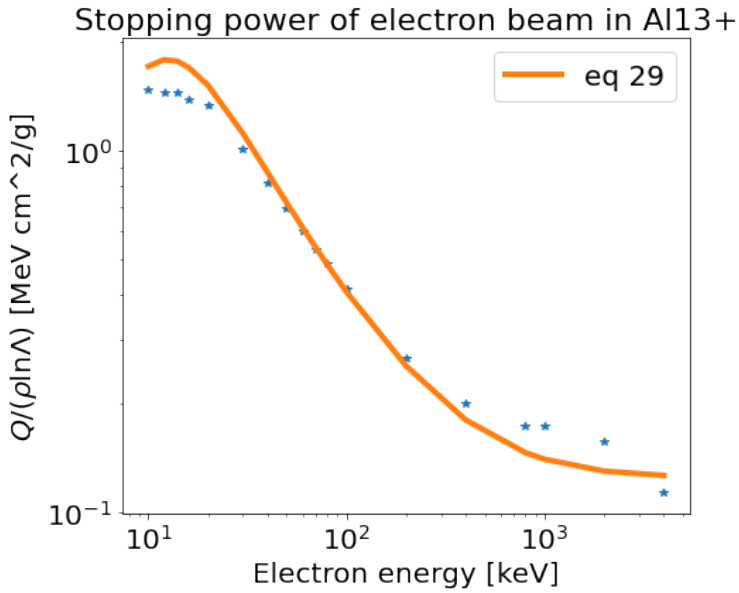

Figure 10: Stopping power calculated in TriForce (blue asterisk) compared to Equation 29 in Perez [8].

Again, there is a good agreement with the analytic expression in Perez et al., validating the collision model used in TriForce for electron-ion collisions. The differences between the analytic model and the calculations are likely due to errors in taking the numerical derivative, $(\frac{dE}{dt})_{|t=0}$ from the data in Figure 9.

3 Conclusions

Electrical conductivity and electron stopping power are important properties of laser generated plasmas and are critical for modeling current and heat flow. The kinetic part of the hybrid fluid-kinetic code TriForce has been used to simulate these properties from first principles. Electrical conductivity in copper has been calculated and

compared with previous analytic work for a range of plasma conditions. The calculated conductivity values compare very well against analytic calculations. Electron stopping power has been tested for electron-ion collisions and it compares favorably with previous calculations. These proof-of-principle calculations indicate that TriForce can be used to predict these microscopic properties for any material, whether in or out of equilibrium. The stopping power was then calculated for an electron beam in aluminum. The calculations using TriForce compare very well with the previously known analytic formula, again indicating that TriForce can be used to model kinetic properties of plasmas very well.

4 Future Work

Future work involves the calculation of conductivity and stopping power for materials of relevance to inertial confinement fusion such as plastic, deuterium, and tritium. These calculations can also be used as inputs for fluid simulations of plasmas. Since this work also indicates that non-equilibrium, non-fluid regimes can be treated accurately with a kinetic model, the particle-in-cell part of TriForce can be used to study kinetic effects in inertial confinement fusion plasmas.

5 Acknowledgements

Thank you to my advisors Mike Lavell and Prof. Sefkow for offering me this project and the huge learning opportunity, not to mention the marathon zoom sessions to help me out as we went along. A huge thank you to Dr. John Shaw for all the help with the code development. Thanks to Dr. Craxton for organizing the program and giving us the opportunity to experience research despite the challenges posed by COVID. Thank you also to Ms. Truebger for coordinating all of our meetings and the Friday Seminars. A huge thank you to all those that made the remote program happen in IT, HPC, and Administration. Lastly, thanks to the other students in the 2021 LLE HS program;

interacting and getting to know them made the program especially enjoyable.

References

[1] E. M. Campbell and W. J. Hogan, "The National Ignition Facility - applications for inertial fusion energy and high-energy-density science", Plasma Phys. Control. Fusion 41, B39 (1999).

[2] T. R. Boehly et al., "Initial performance results of the OMEGA laser system", Opt. Commun. 133, 495 (1997).

[3] J. Nuckolls, L. Wood, A. Thiessen, and G. Zimmerman, "Laser compression of matter to super-high densities: Thermonuclear (CTR) applications," Nature 239, 139 (1972).

[4] J. D. Lindl, "Development of the indirect-drive approachto inertial confinement fusion and the target physics basis for ignition and gain," Phys. Plasmas 2, 3933 (1995).

[5] R. S. Craxton et al., "Direct-drive inertial confinement fusion: A review", Physics of Plasmas 22, 110501 (2015).

[6] S. A. Slutz et al., "Pulsed-power-driven cylindrical liner implosions of laser preheated fuel magnetized with an axial field", Physics of Plasmas 17, 056303 (2010).

[7] A. Sefkow et al., "Introduction to TriForce: A Multiphysics Code for Hybrid Fluid Kinetic Simulations," Bull. Am. Phys. Soc. 64 (2019).

[8] F. Perez et al., "Improved modeling of relativistic collisions and collisional ionization in particle-in-cell codes", Phys. Plasmas 19, 0831904 (2012).

[9] Private communication with S. X. Hu